ISSN-0379-301X

UNIVERSITE LIBRE DE BRUXELLES - VRIJE UNIVERSITEIT BRUSSEL

INTER-UNIVERSITY INSTITUTE FOR HIGH ENERGIES

A MEASUREMENT OF THE TOTAL CHARM PRODUCTION CROSS SECTION IN PP INTERACTIONS AT 200 AND 360 GeV/c

Universities of Brussels
Pleinlaan, 2
1050 Brussel

June 1984
IIHE-84.03

A MEASUREMENT OF THE TOTAL CHARM PRODUCTION CROSS SECTION IN PP INTERACTIONS AT 200 AND 360 GeV/c.

M.T. MUCIACCIA[1)], S. NATALI[1)], S. NUZZO[2)], F. RUGGIERI[2)]
Universita di Bari, Bari, Italy

M. BARTH[5)], H. COBBAERT[6)], D. GEIREGAT[6)], R. ROOSEN[3)], S.P.K. TAVERNIER[3)]
Inter-University Institute for High Energies, Brussels, Belgium

H. DREVERMAN, K. GEISSLER, A. HERVE, E. JOHANSSON, P. LECOQ, P. OLIVIER[4)]
CERN, Geneva, Switzerland

J.H. BARTLEY, F.W. BULLOCK, M. COUPLAND, R. CRANFIELD, D.H. DAVIS, B.G. DUFF, M.J. ESTEN, I. GJERPE, F.F.HEYMANN, P.R. HOBSON, D.C. IMRIE, G. LUSH, D.N. TOVEE, O.R. WILLIAMS
Physics and Astronomy Department, University College, London, England

J.L. BAILLY, J.F. BALAND, F. GRARD, V.P. HENRI, J. KESTEMAN
Universite de l'Etat a Mons, Mons, Belgium

R. ARNOLD, G. MAURER
Division des Hautes Energies, CNRS-Strasbroug, France

H. HRUBEC, G, NEUHOFER, A. TAUROK
Institut fur Hochenergiephysik, Wien, Austria

Submitted to the International Conference on High Energy Physics, Leipzig, July 1984
Session B10 (Production and decay of new particles)

---

1) Dipartimento di Fisica, Universita di Bari
2) INFN Bari
3) Bevoegdverklaard Navorser, NFWO, Belgium
4) Now at Physics Department, Yale University, New Haven
5) Chercheur agrée FNRS, Belgium
6) Vorser IIKW, Belgium

ABSTRACT

The total charm production cross section was measured in pp interactions at 200 and 360 GeV/c. The set up consisted of a holographic heavy liquid bubble chamber HOBC and a muon tirgger. An analysis of part of the data gives for the total charm production cross section : $\sigma = (2.8 \pm 4)\mu b$ and $\sigma = (12.4 \begin{smallmatrix} + 0.4 \\ - 3.7 \end{smallmatrix})\mu b$ at 200 and 360 GeV/c respectively. This indicates a very rapid rise of the cross section with energy. Comparing our data with similar results on hydrogen we obtain for the A dependence of the charm cross section (A^{α}) $\alpha = 0.92 \begin{smallmatrix} + 0.21 \\ - 0.16 \end{smallmatrix}$.

1. INTRODUCTION

In spite of 10 years of continuous and intense efforts, our knowledge of the total charm production cross sections in hadron-hadron collisions is still very unsatisfactory. The uncertainty on the actual value of this cross section at ISR energies ($\sqrt{s} \sim 60$ GeV) still spans an order of magnitude. Moreover no experiment has measured this cross section in proton-proton collisions at different energies with the same apparatus. As a result, its energy dependence, which is important to discriminate between various theoretical proposals, is very poorly determined.

In the experiment described below the total charm production cross section was determined in proton-nucleon interactions at an incident momentum of 200 and 360 GeV/c.

A proton beam was chosen rather than a pion beam because the quark structure functions in the proton are better known and because it allows a comparison to be made with measurements performed in beam dump experiments or with data at higher energies (ISR-data).

2. THE EXPERIMENTAL SET UP

The set up consists of a holographic heavy liquid bubble chamber HOBC and a muon trigger. Figures 1 and 2 show the general layout of the experiment and of the holographic recording scheme.

Upstream of the bubble chamber at 1.655 and 12.347 m are two proportional chambers B1 and B2 with two orthogonal wire planes of 1 mm pitch each. These chambers are essential to localise the interactions corresponding to the trigger in the holographic image. The bubble chamber itself, its holographic recording scheme and the holographic scanning and

measuring tables have been described elsewhere [1, 2, 3, 4]. Below we succincetly describe those aspects which are relevant for the understanding of the results reported.

The active liquid in the bubble chamber is C_3F_8. This liquid has an interaction length of 110 cm and a radiation length of 25cm. The bubbles in a visible volume of 5 x 6.2 x 10 cm^3 are recorded holographically on film. The full width at half maximum of a bubble profile is 10 μm, and, thanks to the holographic recording scheme, the depth of field covers the full depth of the chamber. Only one hologram is recorded per event. The threedimensional properties of a hologram allow to measure all three space coordinates in one image. The coordinate along the optical axis is measured by focussing on a bubble, and the corresponding measurement accuracy is 120μm. The accuracy on the two other coordinates is limited by distorsions in the relay lens used in the recording and is 6μm. The chamber cycling rate was 10 Hz, the bubble density 95 bubbles cm^{-1} and the beam was tuned to 70 particles/expansion.

Immediately behind the bubble chamber, and as close as was practical, are four scintillators (S3) and a massive iron and tungsten dump. Picture taking was triggered by requiring :

a) a good beam particle,
b) an interaction in the chamber signalled by pulse hight in the scintillators S3,
c) a muon signalled by a hit in a scintillator hodoscope H1.

Particles emitted at less than 54 mr from the beam direction had to penetrate 6.5 cm of Cu, 200 cm of tungsten and 39.5 cm of Fe to reach the hodoscope, particles emitted at more than 54 mr had to penetrate 6.5 cm of Cu and 239.5 cm of Fe. This corresponds to a minimum energy for the muon of 6.11 and 3.21 GeV respectively. The angular acceptance of the muons was defined by 9 planes of hexagonal proportional chambers located between the dump and the scintillator hodoscope H1. These accept tracks produced in the target at less than ≈ 100 mr.

The instrumented part of the dump behind the hodoscope plane is not relevant for the present analysis.

Figures 3 and 4 show examples of events observed in the bubble chamber.

3. DATA TAKING AND DATA ANALYSIS

Data were taken at the SPS accelerator at CERN in an unseparated positive secondary beam at 360 and 200 GeV/c. At 360 GeV/c the beam is essentially a pure proton beam, but at 200 GeV/c it contains 76.4% of protons, 21% of π^+ and 2.6% of K^+. The π^+ and proton particles in the beam are tagged with two beam Cerenkov counters (CEDAR's). For the final results interactions on incoming pions are removed from the sample. A total of 23 000 and 17 000 holograms was recorded at 360 GeV/c and 200 GeV/c respectively. The results reported here correspond to 80% of the 360 GeV/c film and 50% of the 200 GeV/c film.

Only holograms which correspond to a trigger with a track in the proportional chambers between the dump and the scintillator hodoscope were analysed (64.5% of the holograms). These are searched for beam particles compatible with the position measured in the beam proportional counters, and producing an interaction in the fiducial volume. The fiducial volume requires at least 2mm of visible incoming beam track and at least 15mm of visible decay path behind the interaction. Such an interaction is found on 42% of the pictures analysed. The procedure selects a wrong interaction unrelated to the muon trigger 4.2% of the time. Of the primary vertices 12% were discarded for various reasons like poor picture quality or ambiguities concerning which vertex belongs to the triggering beam track. The remaining primary vertices were all carefully scanned for any secondary activity. Two independent scans were made and the differences checked on the

scanning table. Any secondary activity in a 2.4 mm wide band extending forward from the vertex to the end of the chamber was recorded. The secondary activities were classified as :

- charged decay candidate of multiplicity n : Kn
- neutral decay candidate of multiplicity n : Vn
- decay candidate of unknown nature (charged or neutral) : Xn
- charged interaction
- neutral interaction
- gamma conversion

A secondary activity is considered to be an interaction if there is either a heavily ionising or a backward track at its vertex. A secondary activity is considered to be a decay candidate if it is not a secondary interaction and if none of the decay tracks shows evidence for multiple scattering. At the level of the scanning we did not require a decay candidate to have the correct multiplicity. Gamma conversions or delta electrons are recognised by their multiple scattering.

For each event with a decay candidate the primary and secondary vertex point were measured accurately; as well as one point on the incoming beam track and one point on each secondary track from the decay vertex. We thus have accurate measurements of all distances and angles in the plane perpendicular to the optical axis. The final sample used in the present analysis contains 3667 and 1276 primary interactions at 360 GeV/c and 200 GeV/c respectively.

4. CHARM PRODUCTION IN EVENTS WITH TWO CHARM DECAY CANDIDATES

In the present experiment evidence for charm production stems from topological information only. It is clear that particular care must be taken to avoid backgrounds from secondary interactions, strange particle decays or γ-conversions which might simulate charm decays. In this respect the muon trigger is essential since it improves the

signal over background ratio by a factor $\sim$ 20. To reduce the background further we require the charm decays to satisfy the transverse distance and the maximum impact parameter cuts listed in table 1 (See figure 5 for a definition of these variables). All distances and angles refer to projected quantities. These cuts are chosen such that only a few procent of the charm decays are removed. In addition it is necessary to require cuts on projected opening angles or decay angles to remove γ-conversions which simulate V2 or K3 decays or to remove electrons where a small amount of multiple scattering could simulate a K1 decay. These angular cuts remove a substantial fraction of the charm decays (see table 1). Figure 6 shows the projected opening angle for V2 decays. The expected distribution for charm decays is also shown. The need for the cut is obvious. Decays satisfying all the cuts of table 1 will be referred to as charm decay candidates.

Even with these cuts most of the charm decay candidates are background. To reduce the background further we restrict our attention to the sample with two charm decay candidates in the same event. In this sample the background can be evaluated under the assumption that the probability that a secondary interaction simulates a charm decay candidate is independent of the fact that there is already such a decay present in the event. In this case the number of events with two (or more) charm decays due to background is given by

$$N_{b,d} = N_T \, [1 - (1 + \varepsilon) \, \mathrm{EXP} \, (- \varepsilon)] \qquad (1)$$

where N_T is the total number of primary interactions analysed, $\varepsilon = N_S/N_T$ and N_S the total number of charm decay candidates. If this formula is applied to samples with little or no charm content, it indeed correctly predicts the number of events with two or more secondary activities (see table 2). Table 3 summarizes the number of events found for different decay topologies with the cuts of table 1. Formula (1) would predict 6.5 doubles at 360 GeV/c (16 observed) and 2.0 doubles at 200 GeV/c (3 observed). There is a clear excess in the 360 GeV/c

data which we attribute to charm production. This procedure however overestimates the background since there is of course a contribution of charm to the singles sample. The excess in the doubles is used to estimate the amount of charm in the singles, which is then subtracted from the singles to evaluate the background in the doubles with formula (1). After a few iterations the procedure converges and the final result is

	doubles observed	expected background
360 GeV/c	16	3.85
200 GeV/c	3	1.7

We conclude that we have a clear evidence for charm production in pp interaction at 360 GeV/c, but hardly any evidence at 200 GeV/c.

5. CROSS SECTIONS

The charm production cross section is given by

$$\sigma(c\bar{c}) = \sigma_{trigger} \frac{N_{cc}}{N_T} \frac{R}{a} A^{\alpha_{inel}-\alpha_{c\bar{c}}} \qquad (2)$$

where $\sigma_{trigger}$ is the triggering cross section (30 mb), $N_{c\bar{c}}$ the number of events with two charm decays attributed to charm, R the fraction of triggering interactions which satisfy the muon requirements, and "a" is the acceptance for charm decays. The factor $A^{\alpha_{inel}-\alpha_{c\bar{c}}}$ accounts for the fact that the atomic number (A) dependence of the charm production cross section ($\alpha_{c\bar{c}}$) may be different from the atomic number

dependence of the total inelastic cross section ($\alpha_{inel} = 0.72$ [5]). The quantity R is an experimentally measured number. It is 0.00457 and 0.00313 at 360 GeV/c and 200 GeV/c respectively. It is in agreement with the trigger rate expected from pion and kaon decay. The trigger acceptance "a" is the product of the trigger acceptance for muons from charm decay a_μ, an acceptance due to the cuts (see table 1) and a visibility factor. The first two factors are calculated by a detailed Monte Carlo calculation. The trigger acceptance a_μ is 0.081 and 0.095 at 200 and 360 GeV/c (assuming no Λ_c production). The visibility factor is essentially a scanning efficiency. We can however not use the usual procedure to determine this scanning efficiency from two independent scans. Indeed, the scanning efficiency goes from essentially zero for very short distance decays to close to 100% at a few mm from the vertex, and the conventional procedure assumes that the probability to see a decay is the same for all the decays. We will assume here that the visibility V is a function of the charm decay length

$$V = V_\infty \ (1 - e^{-\beta L}) \qquad (3)$$

V_∞ represents the scanning efficiency for decays at large distance from the vertex. It is determined from two independent scans of decay candidates satisfying the cuts in table 1 but using only those events with a decay length larger than 5 mm. The result is $V_\infty = 0.95$ after two scans. The parameter β in (3) is determined from a comparison of the decay length distribution for all charm decays occuring in doubles with a decay length distribution generated by Monte Carlo simulation. The Monte Carlo length distribution multiplied by (3) is fitted with a maximum likelihood method to the experimental length distribution. The relevant distributions are shown on figure 7. In this fit the background in the doubles sample is properly taken into account by using the length distribution of the single charm decay candidates, excluding those occuring in doubles, to represent the background. The result is

$$\beta = 0.61 \ ^{+\ 0.75}_{-\ 0.29} \ \text{mm}^{-1}$$

The visibility, averaged over the charm decay length distribution is

$$\langle V \rangle / V_\infty = 0.65 \begin{matrix} + 0.15 \\ - 0.13 \end{matrix}$$

The resulting value for the cross section then is

$$\sigma(c\bar{c}) = 12.4 \begin{matrix} + 4.0 \\ - 3.7 \end{matrix} \mu b \qquad (360 \text{ GeV/c})$$

$$= 2.8 \pm 4 \ \mu b \qquad (200 \text{ GeV/c})$$

Another independent method to determine the charm cross section in our data is to use the length distribution of the charm decay candidates and to assume that the background has a flat and constant distribution in decay length. For this however it is necessary to correct the length distribution for the effect of the transverse distance scanning box cuts, for the finite length of the scanning volume, and for the visibility as defined above. The resulting distribution is shown on fig. 8. There is a clear excess at $L < 18$ mm. Assuming all events above the horizontal line to be due to charm we find an <u>inclusive</u> charm production cross section of

$$43 \begin{matrix} + 14.9 \\ - 8.5 \end{matrix} \mu b$$

The result is in fair agreement with the charm pair production cross section determined previously. We regard the first result however as more reliable.

6. DISCUSSION AND CONCLUSIONS

We have determined the charmed pair production cross section and the inclusive charm production cross section in proton-nucleon collisions at 200 and 360 GeV/c to be 2.8 ± 4 μb and $12.4 \pm^{4.0}_{3.7}$ μb respectively if linear A dependence is assumed. The values quoted depend on a detailed simulation of the characteristics of charm production and decay. We checked however that the result does not depend on any reasonable change of the parameters in the Monte Carlo calculation, except for the semi-leptonic branching ratios and the lifetimes of the charmed particles. Both quantities are reasonably well known from other experiments [7,8]. The average semileptonic branching ratio used was 11% and the lifetimes were taken from ref. [8]. The errors quoted on the cross sections do not include the uncertainties or errors on these quantities. The most serious uncertainty in our result is caused by possible Λ_c production. The sensitivity of this experiment to (Λ_c, $\bar{D}$) final states is suppressed because of the smaller semileptonic branching ratio of the Λ_c (which is however poorly known) and the smaller Λ_c lifetime which results in a smaller visibility for the Λ_c. Strictly speaking, the quantity which we have measured in the doubles analysis is

$$\sigma(\text{charmed meson-antimeson}) + 0.52\ \sigma(\Lambda_c\text{-antimeson})$$

This is the first experiment where the charm production cross section in proton-proton collisions is determined with the same set up at two different energies. The systematic errors in our result should not affect the ratio of the cross section. We obtain

$$\frac{\sigma(360\ \text{GeV/c})}{\sigma(200\ \text{GeV/c})} = 4.4 \pm 2.8$$

This shows a very rapid increase of the charm production cross section with energy. Figure 9 compiles the charm production cross sections in proton-proton interactions at different energies. Such a rapid change is expected in model calculations[9,10]. A comparison of our result with the charm production cross section on hydrogen[6] favours a linear A dependence for the total charm production cross section. Combining both results we get

$$\sigma_{c\bar{c}} = 0.92 \begin{matrix} + 0.21 \\ - 0.16 \end{matrix}$$

REFERENCES

1. A. Herve, K.E. Johansson, P. Lecoq, P. Olivier, J. Pothier, L. Veillet, G. Waurick and S.P.K. Tavernier Nucl. Instr. and Methods, 202 (1982) 412

2. J.L. Benichou, A. Herve, K.E. Johansson, P. Lecoq, P. Olivier, J. Pothier, G. Waurick, E. Wiatrowski, R. Roosen, S.P.K. Tavernier, G. Van Beek and O.R. Williams Nucl. Instr. and Methods, 214 (1983) 245

3. S.P.K. Tavernier; Holographic image recording in visual particle detectors - Proceedings of the 2nd Pisa Conference on New Particle Detectors (1983); To be published in Nucl. Instr. and Methods

4. M. Barth, J.J. Dumont, R. Goorens, R. Roosen, S.P.K. Tavernier, G. Van Beek and G. Wilquet; A scanning table for holographic bubble chamber or streamer chamber images; to be published in Nucl. Instr. and Methods

5. A. Carrol et al.; Phys. Lett., 80B (1979) 319

6. M. Aguilar-Benitez et al.; Phys. Lett., 135 (1984) 237

7. M. Scheider; Semileptonic decays of c and b quarks; Brighton Conference, Brighton 1983

8. G. Kalmus; Weak decays of new particles; Proceedings of the 21th International Conference on High Energy Physics, Paris, July 1982

9. B.L. Combridge; Nucl. Phys., B151 (1979) 429

10. R. Odorico; Moriond Workshop on new flavours, 1982

TABLE 1 : Cuts which define a charm decay candidate. The loss in charm decays (in %) for each cut considered separately is given. The acceptance is the combined effect of all the cuts. The acceptance averaged over all topologies is given for two values of the visibility parameter β, all other numbers in this table correspond to $\beta = \infty$. In the Monte Carlo calculation it was assumed that all charm is produced is meson-antimeson pairs. If all final states are $\Lambda_c \bar{D}$ the results are very similar; e.g. the average acceptance for $\beta = 0.61\ mm^{-1}$ is 0.69 .

K1	$L_T < 500\ \mu m$	1.2
V2	$L_T < 300\ \mu m$	0.8
K3	$L_T < 500\ \mu m$	1.4
V4	$L_T < 300\ \mu m$	0.5
K1	$L \sin\theta_D < 1000\ \mu m$	1.8
V2	$[L \sin\theta_D]_{max} < 1000\ \mu m$	0.4
K3	$[L \sin\theta_D]_{max} < 2000\ \mu m$	0.5
V4	$[L \sin\theta_o]_{max} < 1000\ \mu m$	0.6
K1	$\theta_{decay} > 10$ mr	39.9
V2	$\theta_{open} > 10$ mr	22.0
K3	$\theta_{open} > 5$ mr	2.3
V4	$\theta_{open} > 5$ mr	1.0
Acceptance	K1	0.58
	V2	0.77
	K3	0.96
	V4	0.985
Acceptance averaged over all topologies	0.74	$\beta = \infty$
	0.69	$\beta = 0.61 mm^{-1}$

TABLE 2 : Number of events with two or more secondary activities as predicted by formula (1) compared with the observed number for categories of events which contain little or no charm (360 GeV/c data)

	# doubles observed	# doubles predicted
Interactions	148	162
Decay topologies without charm cuts	317	279

TABLE 3 : Summary of the numbers of events in different categories

		200 GeV/c	360 GeV/c
Total number of primary vertices analysed		1276	3667
Number of charm decay candidates of topology	K1	46	116
Idem	K3	9	25
Idem	V2	11	42
Idem	V4	0	2
Idem	X1, X2, X3, X4	6	38
Number of events with two or more charm decay candidates		3	16

FIGURE CAPTIONS

Fig. 1 : Layout for the holographic image recording

Fig. 2 : General layout of the experiment : B1 and B2 are beam defining proportional wire chambers, S1-S3 are scintillation counters, H1-H3 are scintillator hodoscopes and W1-W7 are proportional wire chambers.

Fig. 3 : Example of a charm candidate. The event contains a K1 and K3 decay at 8.90 and 12.14 mm from the main vertex. The picture is a computer generated perspective view. Angles and distances are non-linearly distorted. The K1 kink angle is 2.7 , and the K3 opening angle is 1.1 .

Fig. 4 : Example of a V4 decay. The picture is again a computer generated perspective view.

Fig. 5 : Definition of the variables transverse decay distance (L_T) and maximal impact parameter $[L \sin\theta_D]_{max}$

Fig. 6 : V2 projected opening angle for a subsample of the 360 GeV/c data. The solid line is a prediction of this distribution for D decays. It is clear that a 10 mr cut will improve the signal to noise ratio in the decay candidate sample.

Fig. 7 : Projected decay length distribution for charm decay candidates occuring in events with two decay candidates and Monte Carlo calculation for the same quantity averaged over the different charm decay modes. The difference is attributed to the visibility of the charm decays.

Fig. 8 : Number of charm decay candiates as a function of decay length for the 360 GeV/c data. The events in this plot have substantial weights and should not be compared directly to table 2.

Fig. 9 : A compilation of total charm production cross sections in proton-proton interactions at different energies. The curves are model predictions : (1) ref.9, charm creation only, m_c = 1.3 GeV; (2) ref.9, charm creation and charmexitation, m_c = 1.3 GeV; (3) ref.10

TABLE 1 : Cuts which define a charm decay candidate. The loss in charm decays (in %) for each cut considered separately is given. The acceptance is the combined effect of all the cuts. The acceptance averaged over all topologies is given for two values of the visibility parameter β, all other numbers in this table correspond to $\beta = \infty$. In the Monte Carlo calculation it was assumed that all charm is produced is meson-antimeson pairs. If all final states are $\Lambda_c \bar{D}$ the results are very similar; e.g. the average acceptance for $\beta = 0.61\ mm^{-1}$ is 0.69.

K1	$L_T < 500\ \mu m$	1.2
V2	$L_T < 300\ \mu m$	0.8
K3	$L_T < 500\ \mu m$	1.4
V4	$L_T < 300\ \mu m$	0.5
K1	$L \sin\theta_D < 1000\ \mu m$	1.8
V2	$[L \sin\theta_D]_{max} < 1000\ \mu m$	0.4
K3	$[L \sin\theta_D]_{max} < 2000\ \mu m$	0.5
V4	$[L \sin\theta_o]_{max} < 1000\ \mu m$	0.6
K1	$\theta_{decay} > 10$ mr	39.9
V2	$\theta_{open} > 10$ mr	22.0
K3	$\theta_{open} > 5$ mr	2.3
V4	$\theta_{open} > 5$ mr	1.0
Acceptance	K1	0.58
	V2	0.77
	K3	0.96
	V4	0.985
Acceptance averaged over all topologies	0.74	$\beta = \infty$
	0.69	$\beta = 0.61 mm^{-1}$

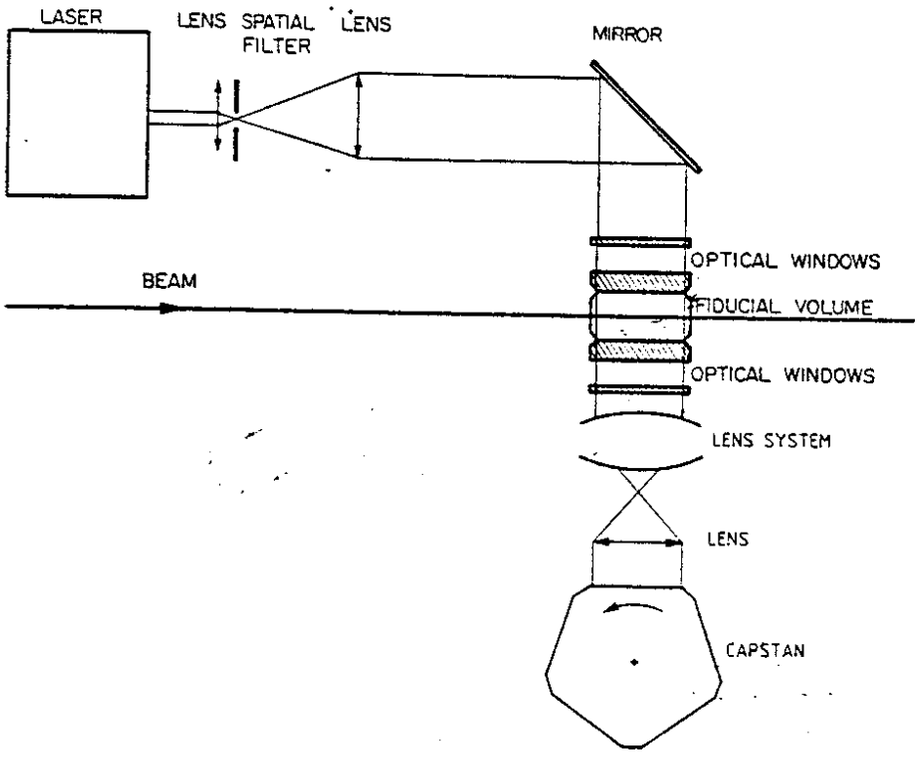
LASER
LENS
SPATIAL FILTER
LENS
MIRROR
BEAM
OPTICAL WINDOWS
FIDUCIAL VOLUME
OPTICAL WINDOWS
LENS SYSTEM
LENS
CAPSTAN

Fig. 1

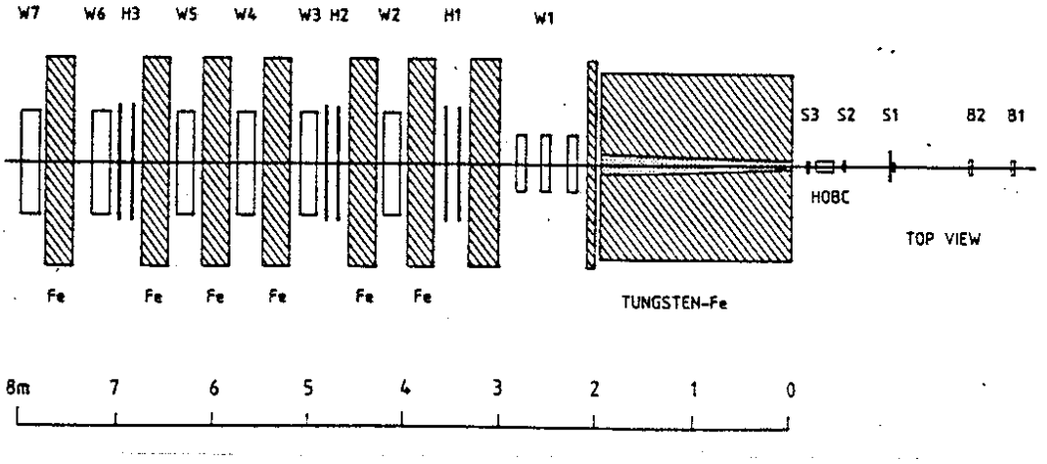
W7
W6
H3
W5
W4
W3
H2
W2
H1
W1
S3
S2
S1
B2
B1
HODC
TOP VIEW
Fe
Fe
Fe
Fe
Fe
Fe
TUNGSTEN-Fe
8m
7
6
5
4
3
2
1
0

Fig. 2

fig 3

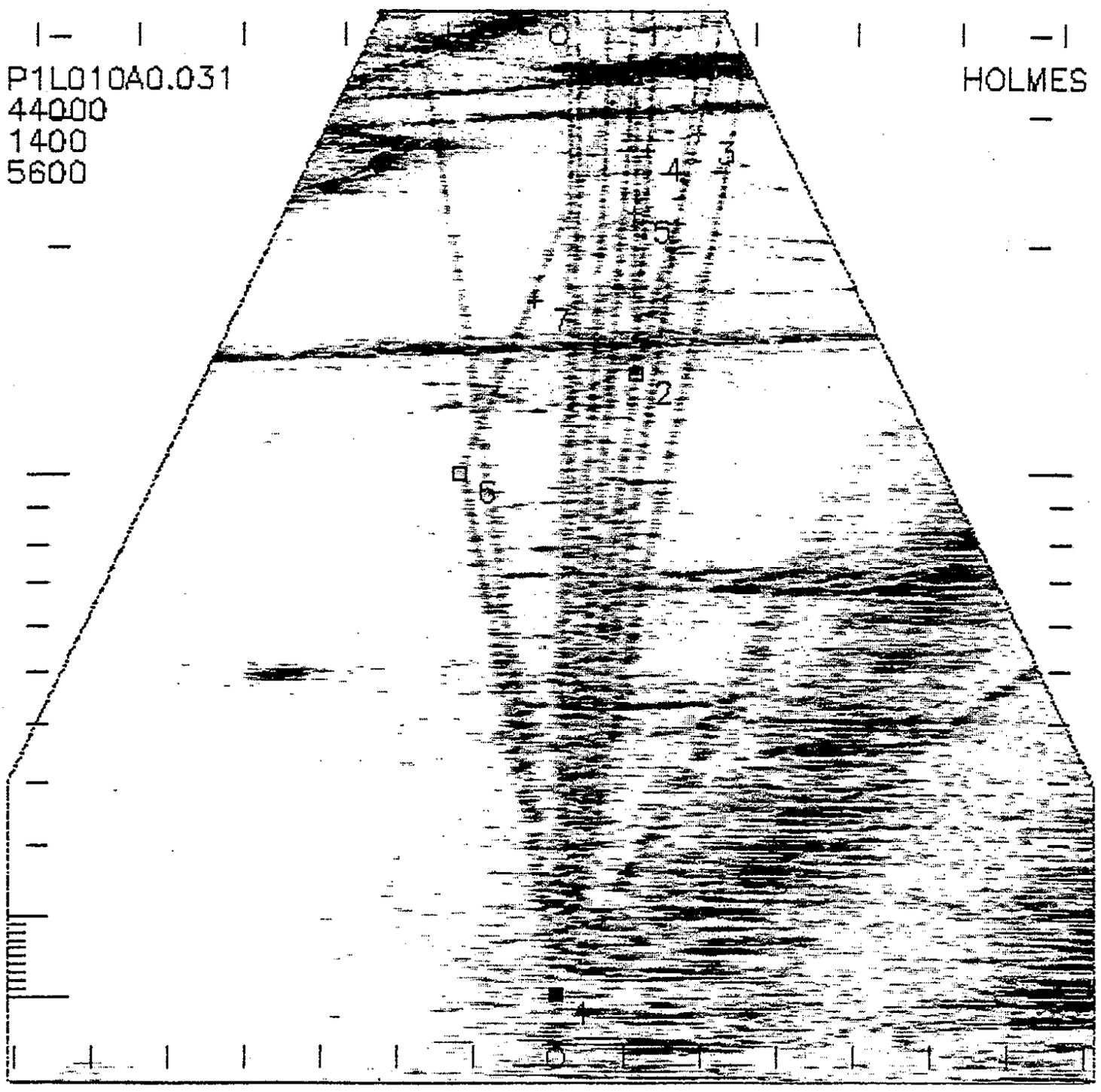

fig 4

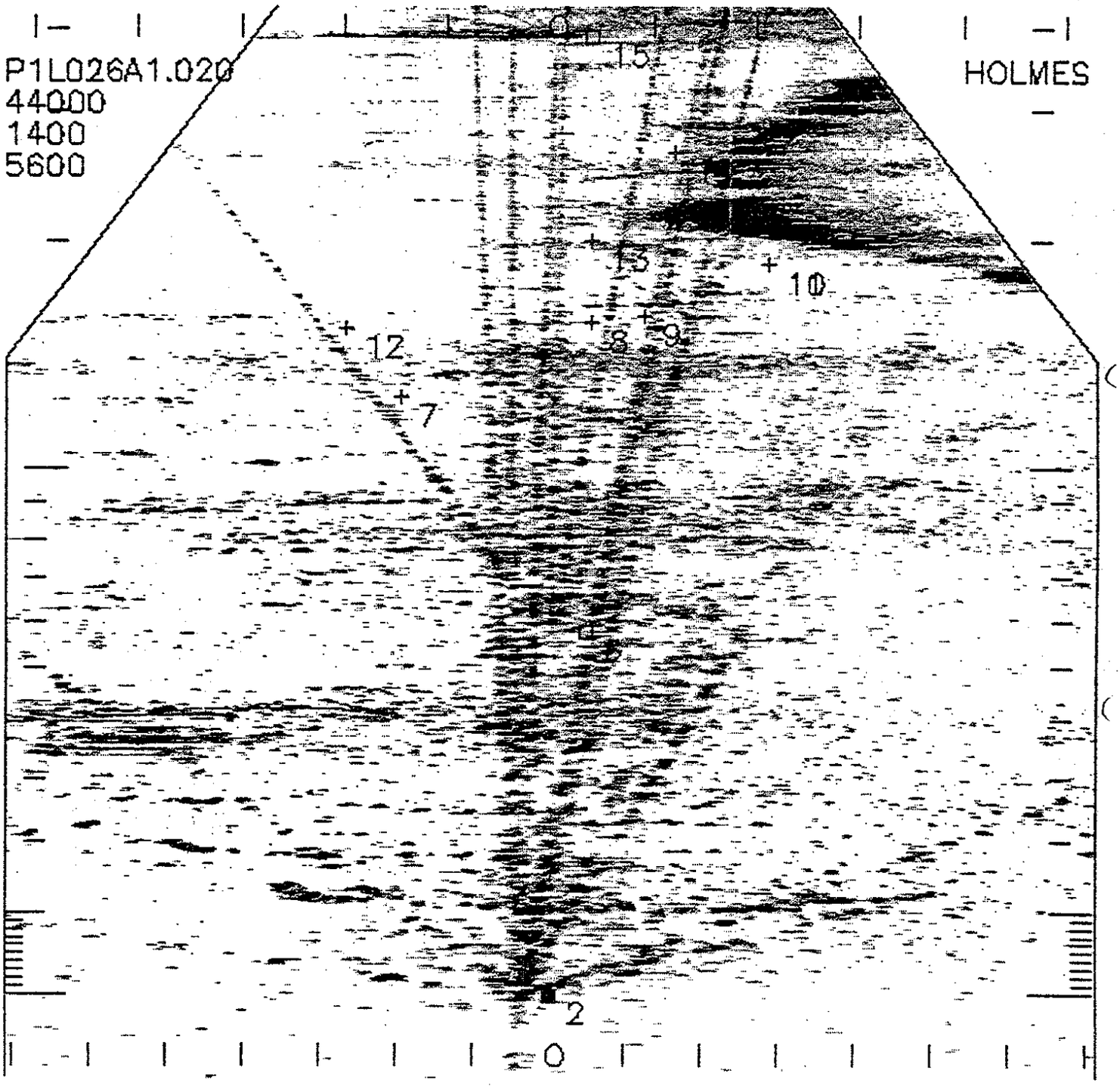

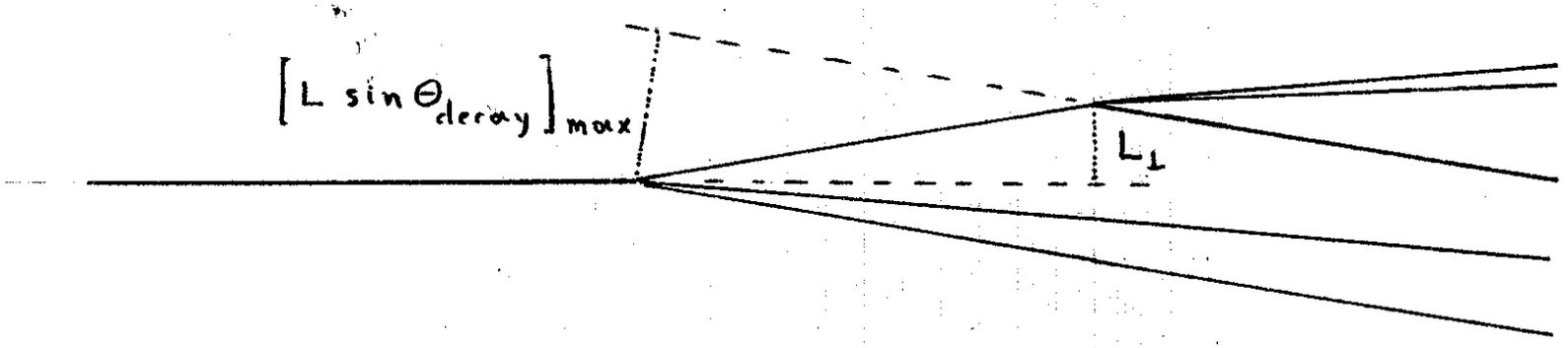

fig 5

Fig. 6

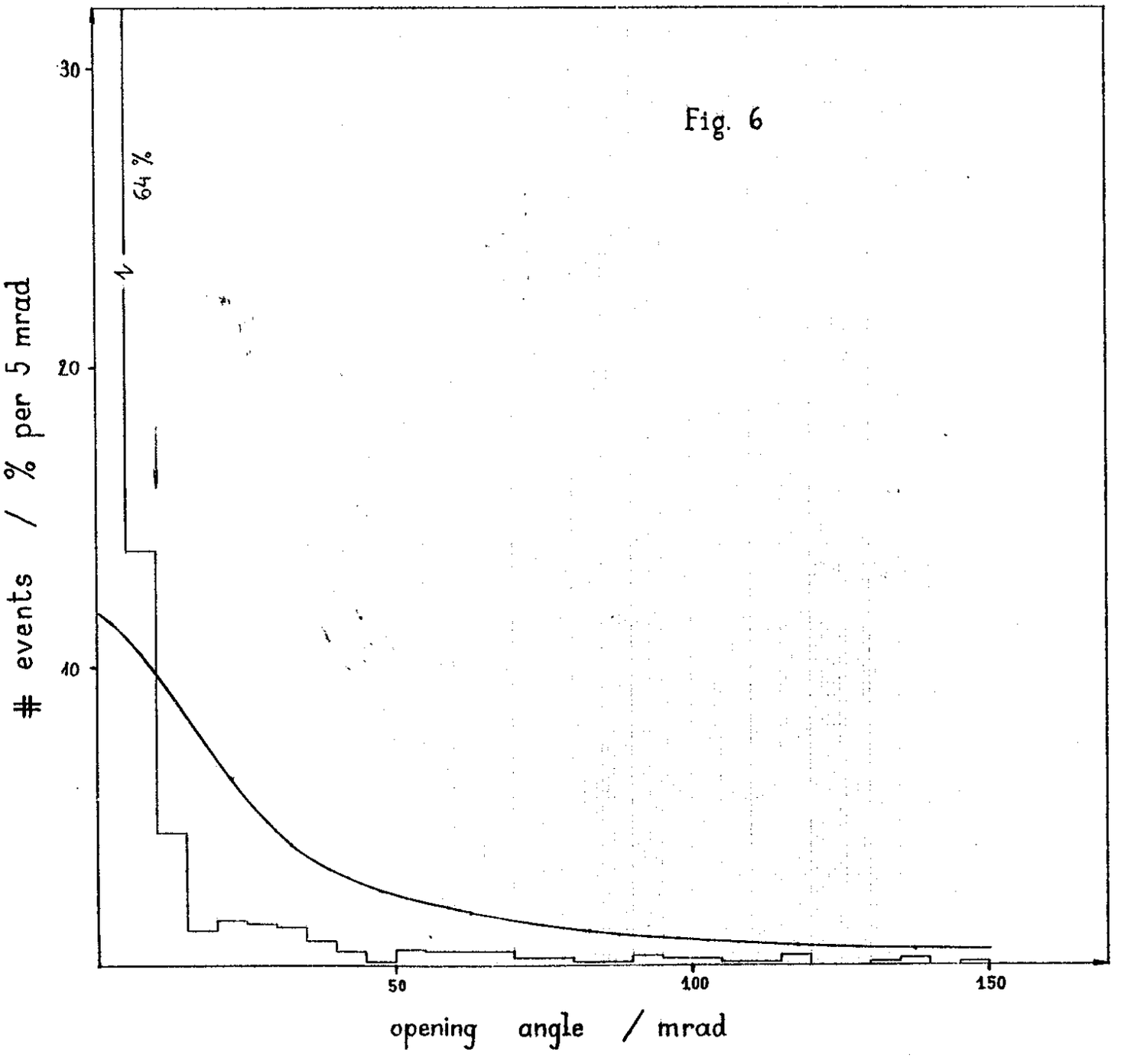

fig. 7

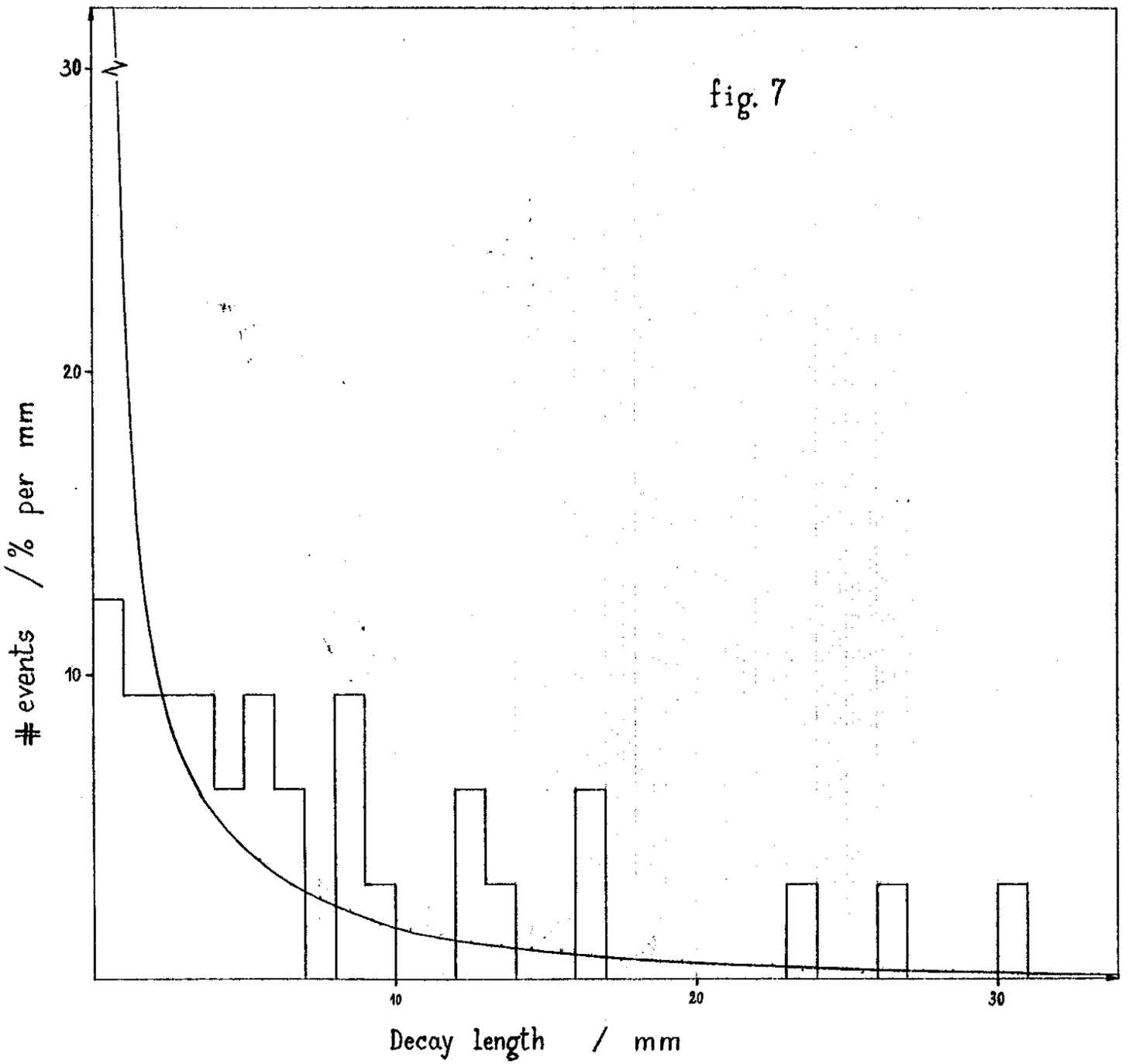

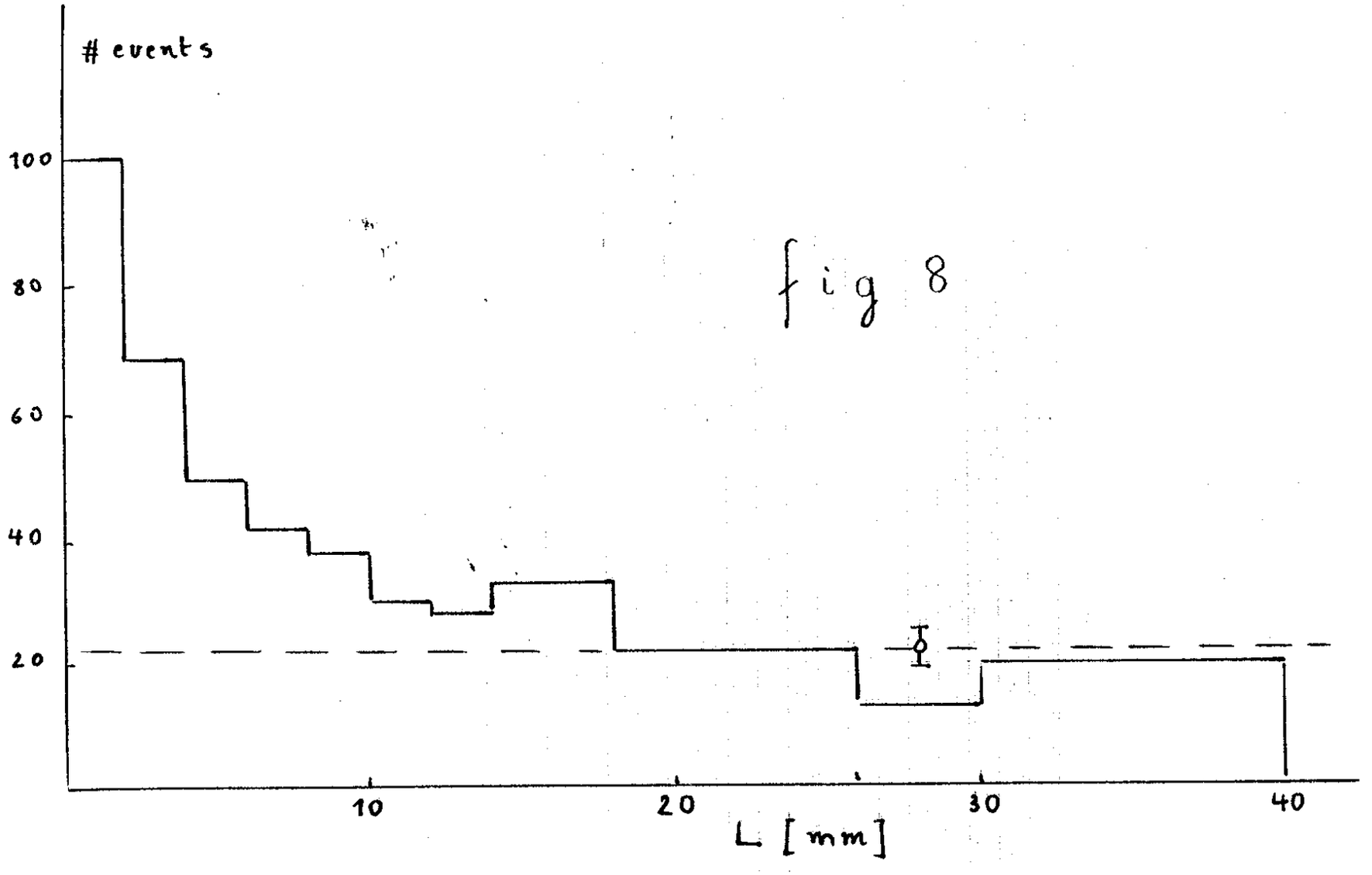

fig 8

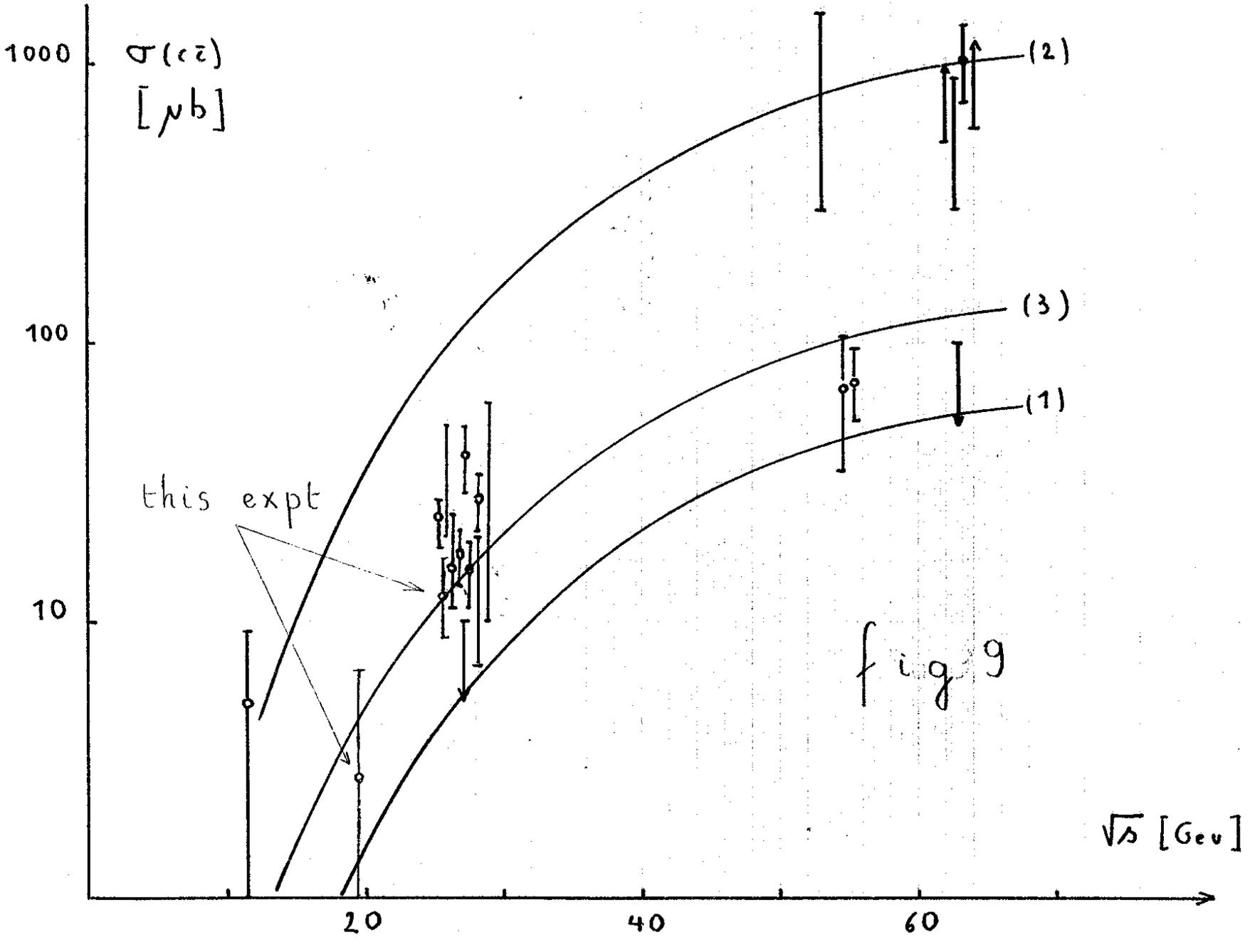

fig 9